Nanostructural Evolution of Sugarcane Rind and Pith Submitted to Hydrothermal Pretreatments

Marcelo M. Oliveira[1,2], Antônio A. S. Curvelo[2,3] and Carlos Driemeier[1]*

[1]*Brazilian Bioethanol Science and Technology Laboratory (CTBE), Brazilian Center for Research in Energy and Materials (CNPEM), Caixa Postal 6192, 13083-970, Campinas, São Paulo, Brasil*
[2]*São Carlos School of Engineering (EESC), University of São Paulo (USP), Caixa Postal 780, 13560-970, São Carlos, São Paulo, Brasil*
[3]*São Carlos Institute of Chemistry (IQSC), University of São Paulo (USP), Caixa Postal 780, 13560-970, São Carlos, São Paulo, Brasil*

Received January 26, 2017; Accepted July 26, 2017

ABSTRACT: Lignocellulose conversion into cellulosic ethanol and coproducts starts with a pretreatment step. Most current industrial plants of cellulosic ethanol use thermochemical pretreatments under hydrothermal conditions, with or without addition of acid catalyst. Such pretreatments modify biomass chemistry and morphology, particularly at the nanoscale. In this work, we use X-ray diffraction, dynamic vapor sorption and calorimetric thermoporometry to investigate the biomass nanostructural changes promoted by hydrothermal conditions. We compare and differentiate the rind and pith fractions of sugarcane stalks in order to contribute to the understanding of rind-pith contrasting recalcitrance. Moreover, for both cane fractions our results point consistently to cellulose co-crystallization, lignin aggregation, and opening of nanoscale pores as the main nanostructural phenomena occurring during hydrothermal treatments.

KEYWORDS: Cellulose, bagasse, sugarcane, cellulosic ethanol, pretreatment

1 INTRODUCTION

Lignocellulosic biomass is a vast, inexpensive renewable resource that can be industrially transformed into materials, chemicals, and liquid fuels. The choice of product mix and process route depends, among other factors, on the biomass feedstock. We are interested in sugarcane biorefineries. About one third of sugarcane dry matter is made of soluble sugars currently used in production of sugar and fuel ethanol [1]. The additional two thirds are lignocellulosic residues: bagasse (the fibrous residues left after crushing the stalks) and straw (leaves and green tops). Bagasse is already gathered at the mill, while straw must be collected from the sugarcane fields. Because sugar-based (1st generation) ethanol is already well established and lignocellulosic residues are available, the Brazilian sugarcane industry is well positioned to lead the large-scale production of cellulosic (2nd generation) ethanol. Once cellulosic ethanol becomes firmly established, the way will be paved for more complex multiproduct biorefineries that harness the vast potential of sugarcane lignocellulose.

The process of cellulosic ethanol production consists of four main steps: pretreatment, enzymatic saccharification, fermentation, and ethanol distillation [2]. Pretreatments are required to reduce the natural recalcitrance (i.e., resistance to deconstruction) of lignocellulosic biomass. Although many pretreatments have been proposed, tested, and shown to be effective [3], so far only a few have been deployed at industrial scale. A recent survey among the pioneering industrial-scale plants of cellulosic ethanol indicated that 5 of the 6 global producers employ either dilute acid or steam explosion pretreatments [4]. Despite differences in equipment design and operation as well as in usage of acid catalyst, these pretreatments actually belong to a common class, with the most fundamental physical chemistry determined by the presence of acidic liquid water at high temperature (140–200 °C). Here we call it the *hydrothermal* conditions present in this whole *class* of pretreatment technologies [5].

Pretreatments modify biomass composition and morphology, and the nanometric scale is especially important. Lignocellulosic biomass is hierarchically structured, from molecules up to macroscopic particles [6]. At the nanoscale, biomass forms fibrillar cellulose

*Corresponding author: carlos.driemeier@bioetanol.org.br

DOI: 10.7569/JRM.2017.6341576

crystallites 3–5 nm wide, laterally associated to form crystallite aggregates, organized in cell wall layers (lamellas) stacked to form micrometric cell walls. Lignin and hemicelluloses are interpenetrated through these levels of the biomass structural hierarchy [7, 8]. In addition to biomass being naturally nanostructured, enzymes have nanometric size [9]. Hence, the enzymatic saccharification performed after pretreatment is essentially the interaction between nanometric biomass components and nanometric enzymes [10].

For investigation of lignocellulose nanostructure, we developed a strategy in which we first improved a set of analytical techniques and then applied them systematically to a wide range of lignocellulosic samples. Our workhorse techniques were X-ray diffraction (XRD) [11], dynamic vapor sorption (DVS) and calorimetric thermoporometry (CTP) [12]. These three techniques probe complementary dimensions of lignocellulose nanostructure. XRD probes cellulose crystallites; DVS, the first hydration layers contacting the polymer matrix; and CTP, pores in the 1–200 nm size range in water-saturated samples. In previous studies, we employed these techniques to investigate nanostructural differences between the rind and pith fractions of sugarcane stalks [13] as well as cellulose co-crystallization [14] and gains in nanoscale porosity [15] upon hydrothermal treatments.

In this work, we generated and characterized a coherent set of samples to jointly investigate the rind-pith differences as well as the nanoscale changes promoted by hydrothermal treatments. We revisit the aforementioned previous studies, which are here discussed in light of the present knowledge. Hence, we provide new data and an updated review of the nanoscale phenomena relevant for lignocellulose biorefineries based on hydrothermal pretreatments.

2 MATERIALS AND METHODS

2.1 Sugarcane Fractionation

The aboveground parts of sugarcane plants were kindly provided by Usina Ipiranga de Açúcar e Álcool LTDA, Brazil. Leaves were removed from the stalks, and the stalks were cut near the nodes to separate the internodes (Figure 1). Internodes from the whole stalks were collected. A bench drill was used to perforate the internodes, separating the center (pith) from the ~1 mm thick periphery (rind). The pith fraction was compressed in a hydraulic press with load of 10 metric tons (distributed in a circular area of diameter 5.4 cm) for 5 minutes to remove sugarcane juice and then exhaustively washed with distilled water to remove residual sugars. The rind fraction was extracted in a soxhlet system with n-hexane to remove wax as well as other extractives and then washed with distilled water. The washed rind and pith fractions were air dried up to 10% moisture content.

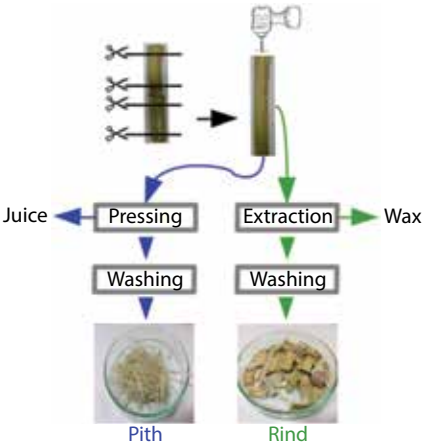

Figure 1 Separation of rind and pith fractions from sugarcane internodes.

2.2 Hydrothermal Treatment and Delignification

Hydrothermal treatments were performed in a 195 mL stainless steel (304 grade) batch reactor heated in a thermostatic glycerol bath. Treatments were performed with 1:10 (w/v) solid-liquid ratio, at 180 °C, for 1 hour. This is a process-relevant condition, which solubilizes most of the hemicelluloses but only a small fraction of the cellulose from bagasse [14]. The reactor was cooled in an ice-water bath and reactor content was filtered and washed until neutral pH. Washed solids were air dried up to ≈10% moisture content.

Delignification was conducted to selectively remove residual lignins for the characterization of the hydrothermally treated solids. Delignification was performed by adding 1% (w/w) sodium chlorite and 0.3% (w/w) acetic acid to an aqueous suspension of 2% (w/w) solids. The system was mechanically stirred and heated at 70 °C for 3 hours. At the end of the first and the second hours, 0.12% (w/w) sodium chlorite and 0.04% (w/w) acetic acid were added to the mixture [16]. Delignification was finished by washing the solid with methanol and cold distillated water. The delignified solids were air dried up to ≈10% moisture content.

2.3 Composition Analysis

Biomass chemical composition was determined by performing analytical acid hydrolysis as detailed by Novo *et al.* [17]. Analytical hydrolysis was performed

in two steps: i) 12 mL of sulfuric acid 72% (w/w) was added to 0.8 g (dry basis) of ground sample and the suspension was magnetically stirred at room temperature for 2 hours; ii) the acid mixture was diluted to 3% and autoclaved for 1 hour at 120 °C. Acid-insoluble lignin was determined gravimetrically. The hydrolysate was analyzed by UV-Vis spectroscopy for determination of soluble lignin and by high performance liquid chromatography (HPLC) for quantification of carbohydrates and sugar degradation products.

2.4 X-ray Diffraction

X-ray diffraction (XRD) was performed in transmission geometry with air-dried sample particulates inserted into capillary tubes. The instrument used was a Rigaku UltraX18HF rotating-anode with Cu Kα radiation (λ=1.54 Å), VariMax monochromating optics, and mar345 image plate detector. The two-dimensional XRD powder patterns were calibrated, corrected and then analyzed with the Cellulose Rietveld Analysis for Fine Structure (CRAFS) model [11]. Diffraction peak shape parameters were set as previously fixed [14].

2.5 Dynamic Vapor Sorption

Dynamic vapor sorption (DVS) was performed in a Q5000 SA from TA Instruments. Samples of ~5 mg were initially equilibrated at 50 °C and 95% relative humidity. Relative humidity was decreased stepwise (desorption) until 0%, and then increased stepwise (sorption). Desorption and sorption isotherms were built based on the measured mass at the end of each relative humidity step, having the sample dry mass as the reference. Isotherms are shown as water content (in unit of g water per g dry matter) as a function of relative humidity [12].

2.6 Thermoporometry

Samples for CTP were exhaustively washed and soaked in water to saturate the solids with water. Samples were then inserted into aluminum pans (Tzero®) and sealed with hermetic lids. CTP was performed in a scanning differential calorimeter (DSC) model TA Q200 with autosampler and RCS90 cooling unit. The instrument was programmed to freeze the sample at −70 °C followed by a series of heating ramps, each ramp followed by an equilibration isotherm. The heat flow signal was analyzed to determine the profile of freezing bound water (FBW), given in units of g water per g dry matter. The FBW profiles are cumulative pore size distributions given as a function of pore diameter (~1–200 nm). FBW was determined from the signal of ice melting below 0 °C, with temperature depression caused by nanoscale confinement. Pore diameter d was calculated from the temperature depression (ΔT) of ice melting by the Gibbs-Thomson equation, $d=2K_c/\Delta T$, with K_c = 19.8 nm K. The details of the method are described elsewhere [12, 18].

3 RESULTS

3.1 Chemical Composition

Raw sugarcane rind and pith show similar contents of the main macromolecular components: lignin, hemicellulose, and cellulose (Table 1). The main difference between the tissues is the higher hemicellulose content in pith (31.3%) compared to rind (26.9%), balanced by slightly less lignin in pith than in rind. Hydrothermal treatments primarily hydrolyze and solubilize the hemicellulose fractions, which show up as much lower hemicellulose contents (4.8% and 3.3%) after hydrothermal treatments of rind and pith, respectively (Table 1). Delignification dramatically reduced the lignin contents to 3.3% and 2.9%, demonstrating the effective removal of lignin from the hydrothermally treated samples.

3.2 X-ray Diffraction

The XRD patterns at the area detector show the characteristic rings coming from cellulose crystallites

Table 1 Chemical composition of raw and treated sugarcane pith and rind.

Treatment	Fraction	Macromolecular contents (%)		
		Lignin	Hemicellulose	Cellulose
raw	Rind	25.4	26.9	48.0
	Pith	23.8	31.3	47.8
hydrothermal	Rind	34.8	4.8	59.9
	Pith	30.5	3.3	55.0
hydrothermal delignified	Rind	3.3	13.4	80.5
	Pith	2.9	8.3	70.6

(Figure 2a), demonstrating that cellulose crystallites are present in the lignocellulosic samples. The experimental two-dimensional patterns are properly fit by the calculation with the CRAFS model (Figure 2b). Cellulose crystallite parameters are determined by the fit. The most pronounced differences are observed in the width of the diffraction peaks associated with lateral dimensions of cellulose crystallites (Figure 2c), and more clearly for the most intense (200) peak. Sharper peaks are interpreted (and modeled by CRAFS) as greater mean crystallite width (Figure 2d). Crystallite width $L_{(200)}$ is greater in raw rind as compared to raw pith, evidencing significant difference between the tissues. Pith also showed greater variability (error bar in Figure 2d), likely reflecting the variable proportions of parenchyma and vascular bundles present in this fraction and illuminated during XRD analysis of the raw pith fraction.

Hydrothermal treatments cause the diffraction peaks to sharpen (Figure 2c). This experimental result is interpreted as increasing mean width of cellulose crystallites (Figure 2d). The underlying phenomenon causing sharper diffraction peaks (and wider crystallites) has been termed co-crystallization [14, 19]. The effects of co-crystallization were more pronounced in pith than in rind, so that the difference observed in raw tissues becomes negligible after hydrothermal treatments (Figure 2d). Delignification promotes slight changes in diffraction peak width, which appear as slightly wider crystallites (Figure 2d). However, such changes due to delignification are too small to support any robust interpretation and it is therefore more appropriate to consider that delignification keeps the crystallites unaltered.

3.3 Dynamic Vapor Sorption

Moisture desorption and sorption in the lignocellulosic samples was investigated with DVS. In this technique, sample mass is monitored continuously while it responds to the programmed relative humidity steps (inset of Figure 3). In the measured sorption isotherms (Figure 3), one observes that water contents are greater in pith than in rind, and greater in raw biomass than in the hydrothermally treated ones. The amount of water measured in sorption isotherms is strongly influenced by crystallite width, with wider crystallites associated with lower water contents [20]. Hence, crystallites wider in rind than in pith (Figure 2d) explains the sorption differences between these raw tissues

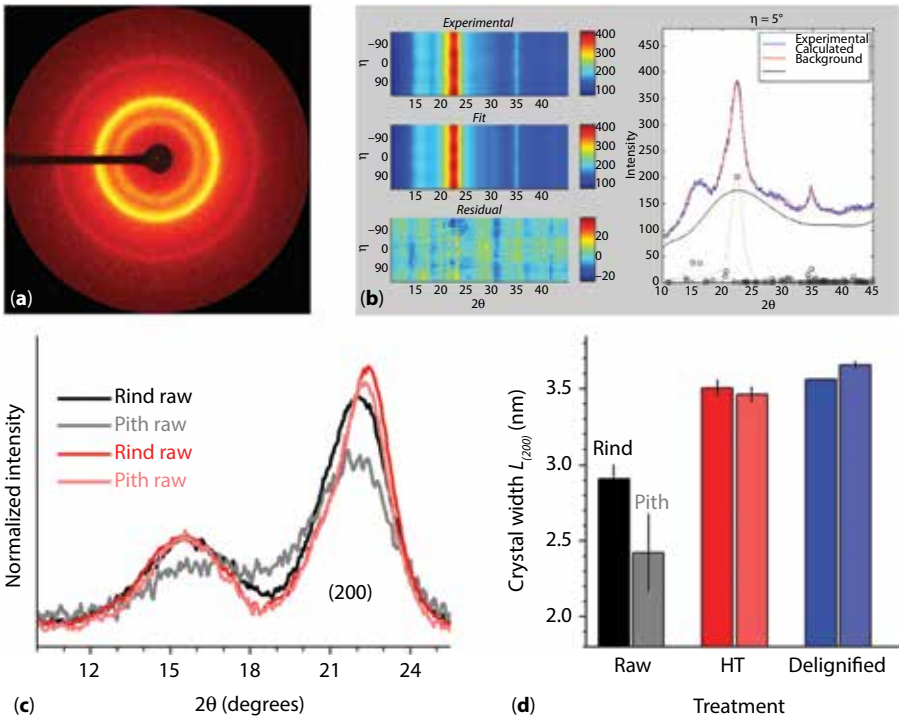

Figure 2 (**a**) Two-dimensional X-ray diffraction pattern acquired from hydrothermally treated sugarcane rind. (**b**) Analysis of the diffraction pattern with the model Cellulose Rietveld Analysis for Fine Structure (CRAFS). (**c**) Background-subtracted diffractograms of raw and hydrothermally treated rind and pith, showing the differences in (200) diffraction peak width. (**d**) Crystallite width $L_{(200)}$ determined from analysis of the diffraction patterns.

(Figure 3). Furthermore, increasing crystallite width due to hydrothermal treatments (Figure 2d) explains the lower moisture sorption in the treated materials (Figure 3). The removal of hemicelluloses in hydrothermal treatments (Table 1) also explains part of the lower moisture gains (Figure 3), but the effect of crystallite width is expected to dominate [20].

3.4 Calorimetric Thermoporometry

The FBW profiles reveal that raw pith has higher nanoscale porosity than raw rind (Figure 4), reproducing the finding from a previous study [13]. Indeed, pith is also more porous than rind after hydrothermal treatment and delignification (Figure 4). Hydrothermal treatment causes substantial gains in nanoscale porosity for both rind and pith, while delignification of the hydrothermally treated samples modifies the shape of the FBW profile. The changing profile shape is summarized by plotting FBW < 4 nm against FBW between 10–200 nm (inset of Figure 4). One observes that hydrothermal treatments promote gains in both ranges of pore size, while delignification promotes FBW gains in the 10–200 nm range, but losses at FBW < 4 nm. This result was observed consistently for other biomass feedstocks and treatment conditions and the signal FBW < 4 nm was shown to be associated with restructured lignin left by the hydrothermal conditions [15].

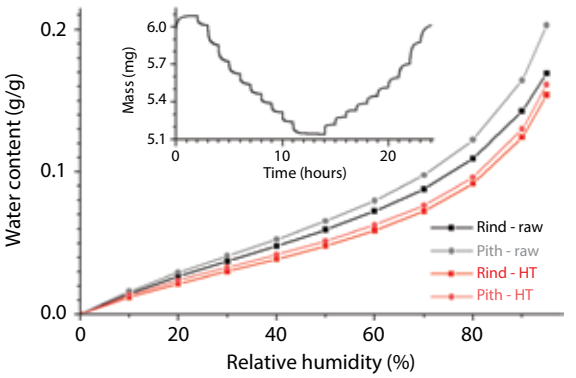

Figure 3 Sorption isotherms obtained by dynamic vapor sorption. The inset exemplifies measured data, where sample mass responds to programmed steps of relative humidity. Desorption (not shown) and sorption isotherms are composed by the mass determined at the end of each relative humidity step referenced to the dry mass determined at 0% relative humidity.

4 DISCUSSION

Rind and pith fractions from the stalk of sugarcane (as well as from other grasses) have shown contrasting recalcitrance (i.e., resistance to degradation), with rind always more recalcitrant than pith. This result has been consistently reported as the distinct tissues have been submitted to thermochemical treatments, *in-vitro* digestibility with fungal cellulases, and incubation with rumen microorganism [21–23]. The contrasting recalcitrance may be explained by several tissue-specific properties: hemicellulose composition and structure [24], cell wall thickness [25, 26], cellulose crystallite width (Figure 2d), as well as water sorption and nanoscale porosity observed in this work (Figures 3 and 4), in agreement with a previous study [13]. Although all these properties may have a role in explaining the contrasting recalcitrance, nanoscale porosity is likely the most critical difference, since nanoscale pores limit the transport of reactants, reaction products and enzymes inside the cell wall. Hence,

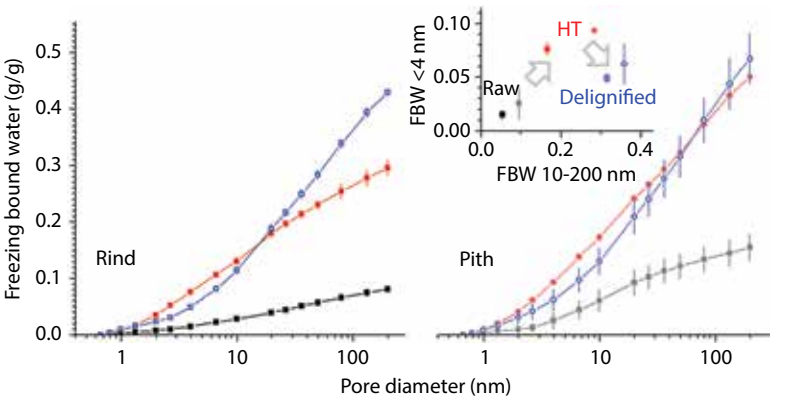

Figure 4 Thermoporometry profiles from rind (left, darker colors) and pith (right, lighter colors) in raw, hydrothermally treated (HT) and delignified states. The inset selects freezing bound water (FBW, in units of g/g) in two ranges of pore diameter (< 4 nm and 10–200 nm), which clusters data points according to their treatment states.

the lower nanoscale porosity of rind compared to pith (Figure 4) deserves to be highlighted.

The increasing cellulose crystallite width in response to thermochemical treatments has been reported for quite a long time in association with wood pulping [27, 28]. However, the mechanisms behind such crystallite dimensional changes have remained elusive. More recently, the phenomenon has attracted a new wave of attention from experimental [14, 19] and theoretical research [29, 30]. The results have indicated that the increasing crystallite lateral dimensions result from the interaction of multiple adjacent cellulose crystallites existing in the raw biomass (co-crystallization). Removal of hemicelluloses acting as intercrystallite spacers is a necessary condition for co-crystallization to occur. In addition, the hydrothermal conditions promote intercrystallite dehydration, favoring the aggregation and fusion of adjacent crystallites [29, 30]. Such fusion of laterally adjacent cellulose crystallites has been proposed as the main mechanism behind the observed gains in mean cellulose crystallite width (Figure 2d).

The hydrothermal conditions also modify the morphology of lignin. Formation of globular lignin aggregates has been observed by electron microscopy [31, 32] and by small-angle neutron scattering [33, 34], which indicated aggregates with radius of gyration of 10–30 nm. Molecular dynamics simulations revealed hydration thermodynamics and promotion of hydrophobic contacts as drivers for lignin aggregation [29]. Moreover, combined molecular dynamics and neutron scattering indicated that the surface of lignin aggregates is irregular and penetrable by probes a few nanometers in size [35]. Hence, water occupying such surface irregularities of lignin aggregates is expected to contribute to the signals measured by calorimetric thermoporometry. Indeed, the signal of FBW < 4 nm was shown i) to positively correlate with the amount of lignin in a set of hydrothermally treated lignocelluloses and ii) to be reduced once the samples are delignified, hence demonstrating the association between lignin and FBW < 4 nm [15]. This calorimetric signature was observed for both rind and pith after hydrothermal treatments (Figure 4), consistent with formation of lignin aggregates in both sugarcane tissues.

Chemical processing can increase the nanoscale porosity of lignocellulosic biomass, as earlier studies have shown for wood pulping [7, 36]. Cell wall fragmentation and delamination (i.e., detachment of wall layers) are likely the primary mechanisms of porosity gain, although lignin and hemicellulose removal and relocation may also contribute significantly. Hydrothermal conditions have also been shown to promote porosity gains, which may be magnified by mechanical action [31, 37]. Enzymes have sizes of ~5 nm [9] and pores larger than that are determinant of enzyme accessibility. Hence, we usually consider FBW in the 10–200 nm range as a good indicator of enzyme accessibility. Our results demonstrate porosity gains in this range of pore sizes (Figure 4). The associated gains in enzyme accessibility are likely the most beneficial alteration promoted by hydrothermal pretreatment.

Pretreatments in cellulosic ethanol production aimed at opening the biomass structure and the observed gains of nanoscale porosity (Figure 4) demonstrate this is indeed an effect of hydrothermal pretreatments. However, cellulose co-crystallization and lignin aggregation are *cohesive* phenomena, contrary to the aim of pretreatments. Hence, although hydrothermal pretreatments do reduce biomass recalcitrance and enhance digestibility, it should be clear that detrimental phenomena co-occur with the beneficial ones. Therefore, as far as alterations in biomass nanostructure are concerned, avoiding the bad as well as promoting the good should be the dual aim for the design of better pretreatments.

5 CONCLUSIONS

Lignocellulose biorefineries should be built on a sound scientific understanding of the phenomena taking place during biomass processing. Nanoscale phenomena are especially important because lignocellulose is naturally nanostructured and the enzymes for biomass deconstruction have nanometric size. In this work, we investigated the nanostructural evolution of sugarcane lignocellulose submitted to hydrothermal conditions typical of the pretreatments employed in the cellulosic ethanol industry. Rind and pith, two sugarcane stalk fractions of contrasting recalcitrance, were characterized by XRD, DVS and CTP. Significant differences between the tissues were observed for all the measured parameters, which help understand the origin of tissue-specific recalcitrance. Moreover, upon hydrothermal treatments, we observed the experimental signatures of cellulose co-crystallization, lignin aggregation, and opening of nanoscale pores that enhance enzyme accessibility. The physical-chemical mechanisms associated with these nanostructural alterations were discussed.

REFERENCES

1. L.A.B. Cortez, *Sugarcane Bioethanol – R&D for Productivity and Sustainability, Blucher*, Blucher, São Paulo (2010).
2. H.B. Aditiya, T.M.I. Mahlia, W.T. Chong, H. Nur, and A.H. Sebayang, Second generation bioethanol production: A critical review. *Renew. Sustainable Energy Rev.* **66**, 631–653 (2016).

3. C.E. Wyman, B.E. Dale, R.T. Elander, M. Holtzapple, M.R. Landisch, and Y.Y. Lee, Coordinated development of leading biomass pretreatment technologies. *Bioresour. Technol.* **96**, 1959–1966 (2005).
4. Novacana, Exclusivo: Custo de produção estimado do etanol celulósico nas 6 maiores usinas do mundo. *Novacana*, 1 (2016).
5. H.A. Ruiz, M.A. Rodríguez-Jasso, B.D. Fernandes, A.A. Vicente, and J.A. Teixeira, Hydrothermal processing, as an alternative for upgrading agriculture residues and marine biomass according to the biorefinery concept: A review. *Renew. Sustainable Energy Rev.* **21**, 35–51 (2013).
6. P. Fratzl and R. Weinkamer, Nature's hierarchical materials. *Prog. Mater. Sci.* **52**, 1263–1334 (2007).
7. J. Fahlén and L. Salmén, Pore and matrix distribution in the fiber wall revealed by atomic force microscopy and image analysis. *Biomacromolecules* **6**, 433–438 (2005).
8. C. Driemeier, Nanostructure of lignocellulose and its importance for biomass conversion into chemicals and biofuels, in *Advances of Basic Science for Second Generation Bioethanol*, M.S. Buckeridge and A.P. de Souza (Eds.), pp. 21–38, Springer, Berlin (2017).
9. C.M. Payne, B.C. Knott, H.B. Mayes, H. Hansson, M.E. Himmel, M. Sandgren, and G.T. Beckham, Fungal cellulases. *Chem. Rev.* **115**, 1308–1448 (2015).
10. J.V. Vermaas, L. Petridis, X. Qi, R. Schulz, B. Lindner, and J.C. Smith, Mechanism of lignin inhibition of enzymatic biomass deconstruction. *Biotechnol. Biofuels* **8**, 217 (2015).
11. R.P. Oliveira and C. Driemeier, CRAFS: A model to analyze two-dimensional X-ray diffraction patterns of plant cellulose. *J. Appl. Crystallogr.* **46**, 1196–1210 (2013).
12. C. Driemeier, F.M. Mendes, and M.M. Oliveira, Dynamic vapor sorption and thermoporometry to probe water in celluloses. *Cellulose* **19**, 1051–1063 (2012).
13. P. Maziero, J. Jong, F.M. Mendes, A.R. Gonçalves, M. Eder, and C. Driemeier, Tissue-specific cell wall hydration in sugarcane stalks. *J. Agric. Food Chem.* **61**, 5841–5847 (2013).
14. C. Driemeier, F.M. Mendes, B.S. Santucci, and M.T.B. Pimenta, Cellulose co-crystallization and related phenomena occurring in hydrothermal treatment of sugarcane bagasse. *Cellulose* **22**, 2183–2195 (2015).
15. C. Driemeier, M.M. Oliveira, and A.A.S. Curvelo, Lignin contributions to the nanoscale porosity of raw and treated lignocelluloses as observed by calorimetric thermoporometry. *Ind. Crop. Prod.* **82**, 114–117 (2016).
16. B.L. Browning, *Methods of Wood Chemistry*, John Wiley & Sons, New York, 1967.
17. L.P. Novo, L.V.A. Gurgel, K. Marabezi, and A.A.D.S. Curvelo, Delignification of sugarcane bagasse using glycerol-water mixtures to produce pulps for saccharification. *Bioresour. Technol.* **102**, 10040–10046 (2011).
18. F.M. Mendes, L.Y. Ling, and C. Driemeier, Laboratory and data analysis procedures for determination of biomass nanoscale porosity employing calorimetric thermoporometry, Technical Memorandum CNPEM (2016).
19. T. Kuribayashi, Y. Ogawa, C. Rochas, Y. Matsumoto, L. Heux, and Y. Nishiyama, Hydrothermal transformation of wood cellulose crystals into pseudo-orthorhombic structure by cocrystallization. *ACS Macro Lett.* **5**, 730–734 (2016).
20. C. Driemeier and J. Bragatto, Crystallite width determines monolayer hydration across a wide spectrum of celluloses isolated from plants. *J. Phys. Chem. B* **117**, 415–421 (2013).
21. H.G. Jung and M.D. Casler, Maize stem tissues: Impact of development on cell wall degradability. *Crop Sci.* **46**, 1801–1809 (2006).
22. M. Zeng, E. Xiemens, M.R. Ladisch, N.S. Mosier, W. Vermerris, C.P. Huang, and D.M. Sherman, Tissue-specific biomass recalcitrance in corn stover pretreated with liquid hot-water: Enzymatic hydrolysis (part 1). *Biotechnol. Bioeng.* **109**, 390–397 (2012).
23. T.H.F. Costa, F. Masarin, T.O. Bonifácio, A.M.F. Milagres, and A. Ferraz, The enzymatic recalcitrance of internodes of sugar cane hybrids with contrasting lignin contents. *Ind. Crop. Prod.* **51**, 202–211 (2013).
24. T.H.F. Costa, M.E. Vega-Sánchez, A.M.F. Milagres, H.V. Scheller, and A. Ferraz, Tissue-specific distribution of hemicelluloses in six different sugarcane hybrids as related to cell wall recalcitrance. *Biotechnol. Biofuels* **9**, 99 (2016).
25. R. Sanjuan, J. Anzaldo, J. Vargas, J. Turrado, and R. Pratt, Morphological and chemical composition of pith and fibers from Mexican sugarcane bagasse. *Holz Roh Werkst.* **59**, 447–450 (2001).
26. C. Driemeier, M.M. Oliveira, F.M. Mendes, and E.O. Gómez, Characterization of sugarcane bagasse powders. *Powder Technol.* **214**, 111–116 (2011).
27. M. Ioelovitch, Zur übermolekularen Struktur von nativen und isolierten Cellulosen. *Acta Polym.* **43**, 110–113 (1992).
28. K. Leppänen, S. Andersson, M. Torkkeli, M. Knaapila, N. Kotelnikova, and R. Serimaa, Structure of cellulose and microcrystalline cellulose from various wood species, cotton and flax studied by X-ray scattering. *Cellulose* **16**, 999–1015 (2009).
29. P. Langan, L. Petridis, H.M. O'Niell, S.V. Pingali, M. Foston, Y. Nishiyama, and B.H. Davison, Common processes drive the thermochemical pretreatment of lignocellulosic biomass. *Green Chem.* **16**, 63–68 (2014).
30. R.L. Silveira, S.R. Stoyanov, A. Kovalenko, and M.S. Skaf, Cellulose aggregation under hydrothermal pretreatment conditions. *Biomacromolecules* **17**, 2582–2590 (2016).
31. L.A. Donaldson, K.K.Y. Wong, and K.L. Mackie, Ultrastructure of steam-exploded wood. *Wood Sci. Technol.* **22**, 103–114 (1988).
32. B.S. Donohoe, S.R. Decker, M.P. Tucker, M.E. Himmel, and T.B. Vinzant, Visualizing lignin coalescence and migration through maize cell walls following thermochemical pretreatment. *Biotechnol. Bioeng.* **101**, 913–925 (2008).
33. S.V. Pingali, V.S. Urban, W.T. Heller, J. McGaughey, H. O'Neill, M. Foston, D.A. Myles, A. Ragauskas, and B.R. Evans, Breakdown of cell wall nanostructure in dilute acid pretreated biomass. *Biomacromolecules* **11**, 2329–2335 (2010).
34. S.V. Pingali, H.M. O'Neill, Y. Nishiyama, L. He, Y.B. Melnichenko, V. Urban, L. Petridis, B. Davison, and P. Langan, Morphological changes in the cellulose and

lignin components of biomass occur at different stages during steam pretreatment. *Cellulose* **21**, 873–878 (2014).
35. L. Petridis, S.V. Pingali, V. Urban, W.T. Heller, H.M. O'Neill, M. Foston, and J.C. Smith, Self-similar multiscale structure of lignin revealed by neutron scattering and molecular dynamics simulation. *Phys. Rev. E* **83,** 61911 (2011).
36. J.E. Stone and A.M. Scallan, A structural model for the cell wall of water-swollen wood pulp fibres based on their accessibility to macromolecules. *Cellulose Chem. Technol*. **2**, 343–358 (1968).
37. P.N. Ciesielski, W. Wang, X. Chen, T.B. Vinzant, M.P. Tucker, S.R. Decker, and B.S. Donohoe, Effect of mechanical disruption on the effectiveness of three reactors used for dilute acid pretreatment of corn stover, Part 2: morphological and structural substrate analysis. *Biotechnol. Biofuels* **7**, 47 (2014).